16TH EUROPEAN CONFERENCE ON EARTHQUAKE ENGINEERING THESSALONIKI 18 - 21 JUNE 2018

TOWARDS A NEW DATASET OF STRONG MOTION RECORDS FROM NEAR-SOURCE REGIONS: PRELIMINARY ANALYSIS

Francesca PACOR,[1] Chiara FELICETTA,[2] Giovanni LANZANO,[3] Sara SGOBBA,[4] Rodolfo PUGLIA,[5] Maria D'AMICO,[6] Emiliano RUSSO,[7] Georgios BALTZOPOULOS,[8] Iunio IERVOLINO[9]

ABSTRACT

The availability of waveforms from moderate-to-strong earthquakes recorded in epicentral areas is a key factor for investigating ground-motion characteristics close to the seismic source and constraining ground motion prediction equations at short source-to-site distances.
To investigate near-source effects on ground-motion, worldwide records were selected from different repositories with the aim of compiling a Near-Source Strong Motion (NSSM05) dataset and the related flat-file of intensity measures and event/station metadata. This dataset consists of more than 1000 manually processed waveforms belonging to 88 events with moment magnitude greater than 5 and recorded in the 1933 – 2016 period. For each NSSM05 event, the corresponding source model and fault geometry were retrieved from literature and catalogues. In order to establish a criterion suitable for representing the near-source condition, and recognize the most relevant features of the ground motion in this region, we considered various distance metrics and performed preliminary statistical analysis of ground motion intensity measures. In agreement with previous studies, it was found that, at short distance from the fault plane (< 5 km) and at long periods (T > 1 s), the fault normal ground motion component is, on average, larger than the fault parallel one, when the intensity is the spectral acceleration. Evidence of directionality effects was also observed at short distances, where the ratio between the maximum value (over all horizontal orientations) of spectral acceleration ordinates and the corresponding median is largest and tends to increase at longer period. Finally, the ratio between the vertical and median values of spectral acceleration is close to unity at high-frequency, while is lower than 2/3 at long periods.

Keywords: strong motion data; source-site distance; seismic source

1. INTRODUCTION

The availability of waveforms from moderate to strong events recorded in epicentral areas is becoming a relevant need for earthquake engineering and engineering seismology purposes. This is demonstrated by the increasing number of studies in the last decades that were focused on the characterization of ground motion effects in the near-source region, particularly after the Izmit Turkey 1999 event (e.g. Campbell and Bozorgnia, 2003; Mavroeidis and Papageorgiou, 2003; Sommerville, 2003; Bray and Rodriguez-Marek, 2004; Chioccarelli and Iervolino, 2010). These studies pointed out that there can be significant differences between seismic ground motions recorded close to and far from the seismic source. It has been observed that such behavior can be responsible for peculiar seismic demand

[1]Francesca Pacor, Istituto Nazionale di Geofisica e Vulcanologia, Milan, Italy, francesca.pacor@ingv.it
[2]Chiara Felicetta, Istituto Nazionale di Geofisica e Vulcanologia, Milan, Italy, chiara.felicetta@ingv.it
[3]Giovanni Lanzano, Istituto Nazionale di Geofisica e Vulcanologia, Milan, Italy, giovanni.lanzano@ingv.it
[4]Sara Sgobba, Istituto Nazionale di Geofisica e Vulcanologia, Milan, Italy, sara.sgobba@ingv.it
[5]Rodolfo Puglia, Istituto Nazionale di Geofisica e Vulcanologia, Milan, Italy, rodolfo.puglia@ingv.it
[6]Maria D'Amico, Istituto Nazionale di Geofisica e Vulcanologia, Milan, Italy, maria.damico@ingv.it
[7]Emiliano Russo, Istituto Nazionale di Geofisica e Vulcanologia, Rome, Italy, emiliano.russo@ingv.it
[8]Georgios Baltzopoulos, Dipartimento di Strutture per l'Ingegneria e l'Architettura, Università degli Studi di Napoli Federico II, Naples, Italy, georgios.baltzopoulos@unina.it
[9]Iunio Iervolino, Dipartimento di Strutture per l'Ingegneria e l'Architettura, Università degli Studi di Napoli Federico II, Naples, Italy, iunio.iervolino@unina.it

imposed on structures. Typical systematic and well known effects observed in the near-source region include relevant vertical component, pulse-like ground motion, permanent displacement (fling-step), hanging/footwall and other effects related to directivity. However, despite the relevant impact of the ground motion characteristics under near-source conditions on the local seismic response, few attempts have been made to properly consider them in seismic code provisions (Grimaz and Malisan, 2014). Among possible factors holding back the development of standard approaches in this field one should probably count the lack of adequate knowledge and/or high level of uncertainty in the characterization of the fault geometry relative to the site and the consequent effects on ground motion.
The aim of this study is to provide a dataset of near-source strong motion records accompanied by high-quality metadata, suitable for seismic response analysis and ground motion studies in proximity to the seismic source. The proposed near source strong-motion dataset (Near-Source Strong Motion dataset v.05, herein called "NSSM05"), collects ground motion parameters and related metadata of worldwide records extracted from various repositories of accelerometric data. The paper describes the criteria adopted to construct NSSM05, that is composed by more than 1000 manually processed waveforms relative to 88 events with moment magnitude greater than 5.0 and the preliminary analysis carried out.

2. COMPILATION CRITERIA OF NSSM05

To construct a dataset of strong-motion waveforms potentially affected by near-source effects, we started by selecting worldwide events according to the following criteria: (1) moment-magnitude (M_w) larger than or equal to 5.0; (2) hypocentral depth up to 40 km; (3) geometrical information on the finite fault model; (4) availability of unprocessed strong-motion waveforms recorded in epicentral area. A criterion to determine the near-source region was found by assuming that near-source effects are more significant when the distance to the fault is less than a few times the fault length. Then, by applying the classical seismological scaling relations (Lay and Wallace, 1995) among seismic moment, slip on the fault and static stress drop $\Delta\sigma$, and the relationship between seismic moment and moment magnitude M_w (Hanks and Kanamori, 1979), the near-source distance R_{ns} has been defined as follows:

$$\log(R_{ns}) < log(k) + (1/3)log(2) + 9.1/3 + (1/2)M_w - (1/3)log(\Delta\sigma) \quad (1)$$

where k is a free parameter used to quantify how many fault lengths the sites should be far from the fault to be considered in near-source region.
According to Equation 1, the near-source distance R_{ns} is dependent on the moment magnitude M_w and the stress drop $\Delta\sigma$ of the event, allowing to generalize the definition of near source region. Figure 1 shows R_{ns} as a function of magnitude assuming k = 2. In this case, the near-source region for magnitude 6.5 and magnitude 7 earthquakes extend up to 50 km and 80 km from the faults, respectively (if the static stress drop is set to 10).

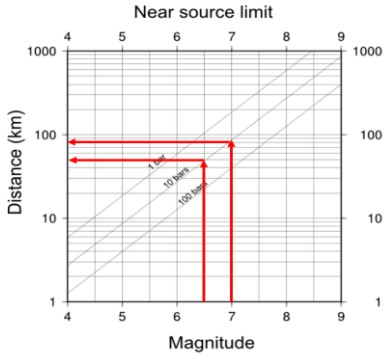

Figure 1. Near-source distance in function of magnitude and stress drop according to Equation 1 with k = 2. The arrows indicate the near-source limits for magnitude 6.5 and magnitude 7 events, setting the stress drop equal to 10.

2.1 Earthquakes and finite fault models

A finite fault model is the key in constructing a flat-file of events-stations metadata and IMs of waveforms recorded in near-source condition. We collected 67 earthquake fault models from published studies or from regional and international databases: Database of Individual Seismogenic Sources (DISS) and Italian Strong Motion Archive (ITACA, Luzi et al. 2016) for Italy; Greek Database of Seismogenic Sources (GreDaSS, http://gredass.unife.it/) for Greece; Engineering strong motion database (ESM; Luzi et al. 2016) and European Strong-Motion Database (ESD; J. Douglas personal communication 2014) for European events; Finite-Source Rupture Model Database (SRCMOD; Mai and Thingbaijam 2014) and NGA-West2 database (Ancheta at al., 2014) for worldwide earthquakes.

For the oldest events, the instrumental hypocenter provided by catalogues may fall beyond the confines of the proposed fault geometry. For this reason, in addition to the coordinates of the instrumental hypocenter, we also included the coordinates of the starting point of the rupture on the fault plane . In cases where the source model did not provide information, we located the nucleation point at mid-length and at 2/3 of the width of the fault, assuming bilateral rupture propagation. We also included 21 events having high-quality strong-motion records in epicentral area, for which we were unable to retrieve complete finite source model information. In these cases, we adopted the strategy of simulating the fault-geometry or some missing parameters in order to calculate several distance metrics. To this aim, we modified the procedure of Kaklamanos et al. (2011), originally developed to convert the different metrics implemented in GMPEs.

The focal mechanism of the events is assigned in accordance to the rake angle of the literature source models or to the solution of the moment tensor provided by the regional and international catalogues, using the convention of Aki and Richards (1980), with the modification of Boore et al. (1997) for strike events.

In total, we collected 88 worldwide earthquakes with moment magnitude greater than 5.0 and hypocentral depth shallower than 40 km, occurred in the period 1933 – 2016. The oldest earthquake is the M_w 6.4 1933 Long Beach event, that contributes only a single record to the dataset, while the most recent are the M_w 8.0, 2016, Kaikoura (New Zealand) event and the M_w 7.0 2016 Kumamoto-shi (Japan) event, that are also the most represented earthquakes with more than 100 waveforms. The majority of the events are located in United State of America (23 events) and Italy (21 events, including the three main shocks of the 2016 central Italy seismic sequence). Japan, Greece and Turkey contribute with about 10 events each. The remaining earthquakes are distributed among Iran (6), New Zealand (6), Montenegro (2), Mexico (1), Nepal (1), Uzbekistan (1) and Chile (1). The largest magnitude of M_w 8.1 corresponds to the 2014 Chile earthquake.

2.2 Source-to-site distance

The un-processed accelerometric time series of the selected 88 events, recorded in free-field condition,

have been collected from a number of agencies managing strong-motion networks around the world. Source-to-site distance of each recording station was calculated using different metrics. We computed the path-term by means of the six source-to-site distance measurements introduced into the NGA-WEST2 database (Ancheta et al., 2014); in addition, we also considered the distance calculated from the coordinates of the nucleation point (R_{NP}) and from the top edge of rupture plane (R_{LINE}).
Table 1 lists the notation and definitions of the adopted source-to-site distance metrics, while Figure 2 provides some examples thereof. In particular, the right panel illustrates the distance R_X defined to be positive for sites on the hanging-wall side of the fault and negative for sites on the footwall side of the fault and the distance R_{Y0}, that is always zero or positive (Kaklamanos et al., 2011).
Furthermore, in order to define a distance metric for which some features of the ground motion are representative of the near-source conditions, independently of the event magnitude, we introduce the *normalized distance* defined as ($R_{NORM} = R_{RUP}/log_{10}L$), where L is the length of the fault in km, and $log_{10}L$ can be considered proportional to the magnitude of the event (Wells and Coppersmith, 1994).

Table 1. Notation and definitions of the distance metrics.

Distance metric	**Description**
R_{EPI}	Epicentral distance: distance from epicentre
R_{HYP}	Hypocentral distance: distance from hypocentre
R_{JB}	Joyner-Boore distance: distance computed from the surface projection of the fault
R_{RUP}	Rupture distance: shorter distance to the rupture plane
R_X	Horizontal distance measured perpendicular to the fault strike, from the top edge of rupture plane
R_{Y0}	Horizontal distance off the surface projection of rupture plane, measured parallel to the fault strike.
R_{NP}	Nucleation distance: distance from nucleation point
R_{LINE}	Shorter distance from the top edge of rupture plane, computed as $\sqrt{R_?^2+R_{?0}^2}$

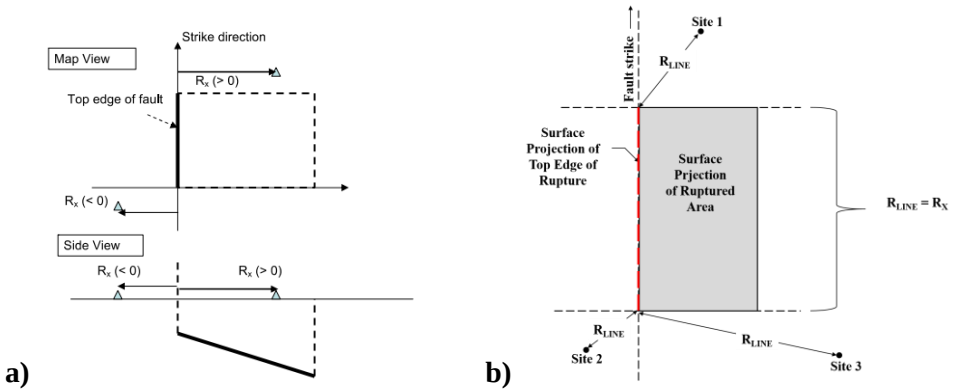

Figure 2. a) map (top) and side (bottom) view of the source-to-site distance measure (R_X) for an example fault (thick black line) plane and stations located on the hanging wall ($R_X > 0$) and footwall ($R_X < 0$) side (taken from Ancheta et al., 2013). b) map view of the source-to-site distance measure R_{LINE} for different sites.

2.3 Near-source strong motion waveforms

To compile the NSSM05 dataset, we selected the ground-motion records located in the near-source region by means Equation 1 with k = 2 and static stress drop equal to 10 bars, that represents an average value for moderate and strong events (Allmann and Shearer, 2009). As distance metric we considered the Joyner-Boore distance such as $R_{JB} \leq R_{ns}$. Applying these criteria, the NSSM05 dataset is composed by 1116 strong motion waveforms (two horizontal and vertical component) from 88 events recorded by 922 accelerometric stations. The choice of selecting data with k=2 is quite

conservative; however, a large dataset allows us to study the distance dependence of peculiar features in near source regions.
The recording sites are classified according to the Eurocode 8, or EC8, classification of subsoil categories (Eurocode 8, 2005), based on the average shear-wave velocity of the uppermost 30 m ($V_{S,30}$). This parameter was inferred from direct measurement of the S-waves profiles, if available. Otherwise, we used geological information or empirical correlation with the topographic slope, as proposed by Wald and Allen (2007). The slope at each station was computed through the Shuttle Radar Topography Mission (SRTM) using the Zevenbergen and Thorne (1987) method assuming a linear relation between shear wave velocity and slope. Table 2 lists the range of $V_{S,30}$ associated to the slope intervals for active crustal regions proposed by Allen and Wald (2009).
As shown in Figure 3, NSSM05 dataset includes 129 stations in class EC8-A (153 records), 442 in class EC8-B (522 records), 296 in class EC8-C (372 records), 14 in class EC8-D (21 records) and 34 in class EC8-E (40 records).

Table 2. Slope and $V_{S,30}$ ranges adopted to classify the near-source recording stations, modified by Allen and Wald (2009).

$V_{S,30}$ range (m/s)	EC8 (EN, 2005)	NEHRP(BSSC, 2001)	Adopted slope range [m/m]
800 – 2000	A	A/B	0.14 – 1
620 – 800	B	C	0.10 – 0.14
490 – 620			0.050 – 0.10
360 – 490			0.018 – 0.050
300 – 360	C	D	$6.3*10^{-3}$ – 0.018
240 – 300			$2.2*10^{-3}$ – $6.3*10^{-3}$
180 – 240			$1.0*10^{-4}$ – $2.2*10^{-3}$
100 – 180	D	E	0 - $1*10^{-4}$

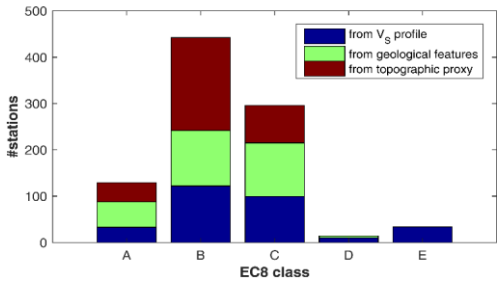

Figure 3. EC8 site classes derived from measured S-waves velocity (V_S) profile (blue), geological information (green) and topographic proxy (dark red).

Waveforms of the NSSM05 were manually processed following the procedure described in Paolucci et al. (2011) and detailed in Pacor et al. (2011). Analog recordings constitute 25% of the NSSM05 dataset; the majority of the digital waveforms are filtered with high pass frequency ≤ 0.1 Hz, whose value tends to decrease with increasing magnitude. Analog data, on the other hand, are generally high-pass filtered at frequencies higher than 0.2 Hz due to their lower quality, with a few exceptions for large magnitude earthquakes. In this way, the statistical analysis can be carried out up to 3s. At longer periods, only digital data should be used or other processing method, based on the baseline correction approach, should be adopted.
Peak ground motion parameters (acceleration – PGA, velocity – PGV, and displacement – PGD), significant duration (T90) and integral parameters (Housner and Arias intensities) are then computed using the corrected waveforms. The 5%-damped acceleration response spectra (SA) values have been calculated for 36 spectral ordinates in the period range 0.01 - 10 s. Additionally, the rotation-independent values RotD50 (the median among all orientations), RotD100 (the maximum), RotD00 (the minimum) as defined in Boore et al. (2010) were evaluated for the following parameters: PGA,

PGV, PGD and 5% damped SA at different periods.
Figure 4a shows the magnitude-distance distribution of the dataset; the number of waveforms in function of magnitude and style of faulting is given in Figures 4b and 4c, respectively. It can be seen that the NSSM05 dataset samples well the 6.5–7.0 magnitude range, the Joyner and Boore distance varies from 0 – 275 km and about two-thirds of the records are within 40 km from the source. Thrust, normal and strike-slip focal mechanisms are well represented in the dataset, while about 2% of the records are associated to oblique focal mechanism.

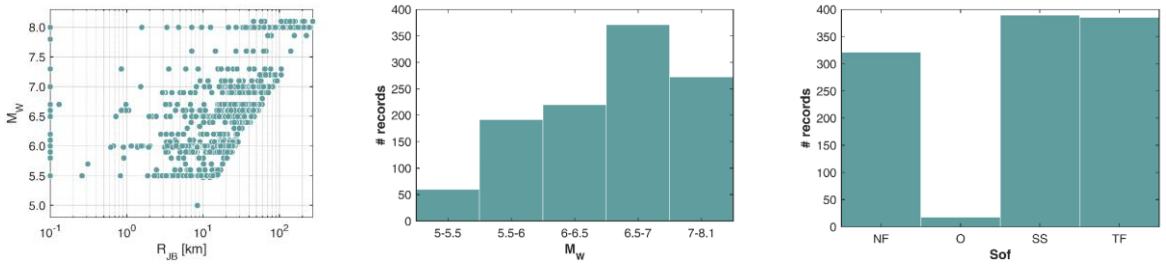

(a) (b) (c)

Figure 4. Distribution of NSSM05 dataset: magnitude (M_w) versus Joyner-Boore distance (a); number of waveforms in function of M_w (b); and style of faulting (c), where NF: normal fault, SS: strike slip fault, TF: thrust fault, O: oblique (right).

Using R_{NORM} metric, the bulk of data is between 0.5 and 40 km and the largest distance covered by the data is 120 km. Comparing R_{RUP} and R_{NORM} with respect to R_{JB} (Figure 5), it can be noted that the largest difference between the metrics is up to R_{JB} 40 km and 100 km, respectively. R_{NORM} and even more R_{LINE} have a larger degree of variability than R_{RUP}, especially at Joyner and Boore distances shorter than 10 km.

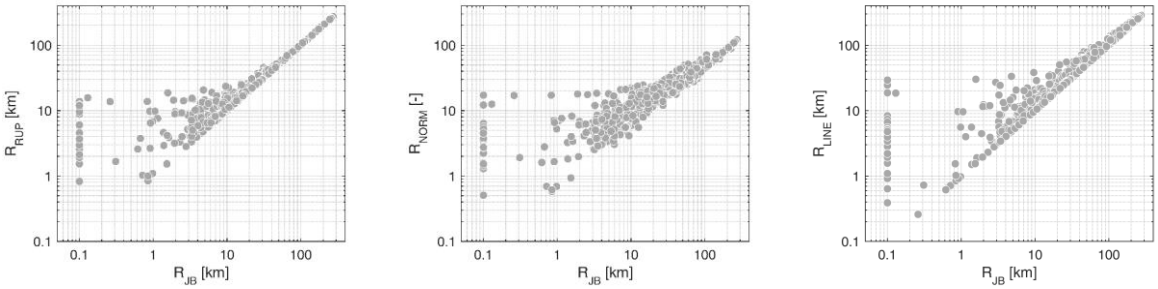

(a) (b) (c)

Figure 5. Rupture distance R_{RUP} (a), normalized rupture distance R_{NORM} (b), line distance R_{LINE} (c) versus Joyner and Boore distance.

3. STATISTICS ON INTENSITY OF NEAR-SOURCE GROUND MOTIONS

In this section, some features of the near-source NSSM05 dataset are discussed. These arise from the statistical analyses of IMs of ground motions (PGA, PGV and 5% damped SA at different periods) calculated from the corrected waveforms and from the distribution of extreme values population.
Since directional effects may be significant close to the seismic source, we adopted different IMs on the horizontal plane. These are: the fault normal (FN) and fault parallel (FP) components calculated rotating the horizontal waveforms according to the strike of the fault; the geometric mean (GM) computed using the two orthogonal components of the recorded ground motion; the maximum (D100), the minimum (D000), and the median (D50) values of IMs over all orientations (Boore 2010).
Figure 6 shows the cumulative distribution of D100 for PGA (a) and PGV (b) of all records of the NSSM05 dataset (gray lines). Black lines represent the lognormal distributions with mean and standard deviation calculated from the data. The median PGA and PGV are 125 cm/s^2 and 12.4 cm/s

respectively, while the 75th percentiles are equal to 236 cm/s^2 and 22.6 cm/s respectively. Following previous studies (Anderson et al., 2013; Pacor et al., 2011), we recognized the extreme waveforms of the dataset as those having PGA ≥ 603 cm/s^2 or PGV ≥ 53.3 cm/s, corresponding to the 95th percentile of the related distributions.

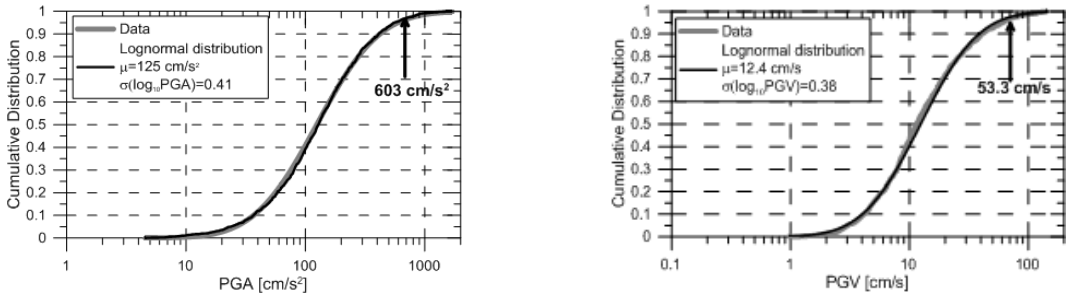

(a) (b)

Figure 6. Distribution of D100 PGA (left) and PGV (right) of NSSM05 dataset (gray lines). Black lines represent the lognormal distributions for mean and standard deviation inferred from data. The arrows highlight the values separating the upper 5th percentiles.

With the proposed criteria, 90 records have been identified. These are almost all relative to the Japanese, Italian and New Zealand events and are observed mainly close to fault. The rupture distance varies from 0.8 – 100 km, although the majority is recorded at distance less than 30 km and covers the entire magnitude range of the dataset (Figure 7). Moreover, no dependence on magnitude and distance is observed for the largest PGA and PGV, suggesting that other physical parameters control these strong amplitudes, possibly directivity, stress drop, site amplification, and others.

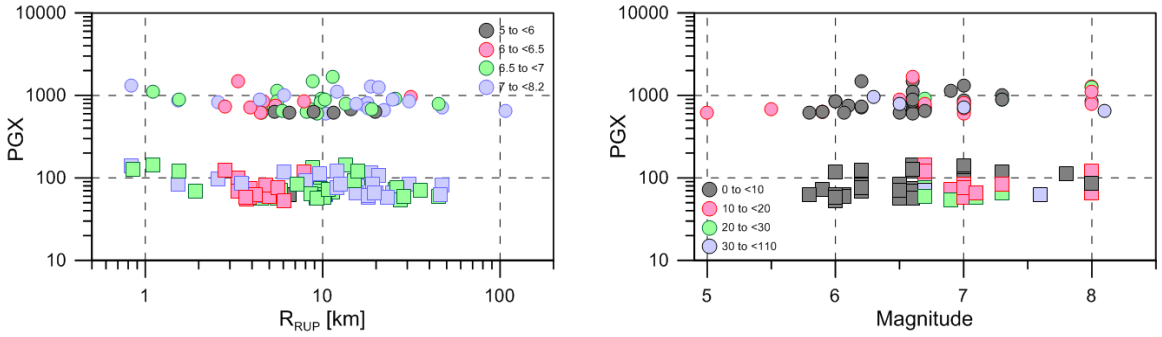

(a) (b)

Figure 7. Extreme PGAs (circles, in cm/s^2) and PGVs (squares, in cm/s) as functions of rupture distance (a) and moment magnitude (b).

3.1 Ground motion components

Figure 8 shows the PGA and the SA (at different vibration periods, T) cumulative distributions of NSSM05 waveforms at periods of 0.3, 1.0 and 3.0 s, recorded at distances < 5km, for FN, FP and vertical (V) components. Note that the number of data varies among adopted metrics.

Regarding the adopted metric, the three ground motion components have similar amplitudes in terms of PGA for values in the upper 40th percentile; conversely, at intermediate and long periods, the 50th percentile of vertical component is about half of the horizontal ones. Difference between FN and FP amplitudes are slight and can be appreciated only at long periods (3s), where FN is about 1.5 FP. At longer distances, this ratio tends to unit, although the dispersion around the mean value decrease with frequency.

In Figure 9, the ratio log_{10} *V/D50* is plotted as a function of R_{RUP}, R_{NORM} and R_{LINE} for PGA and SA at T = 1.0 s and 3.0 s, to better describe the behaviour of the vertical ground-motion at short,

intermediate and long periods. *V/D50* is significantly dependent on period and distance, as observed by previous authors (Bozorgnia and Campbell, 2004; Bindi et al., 2011; Bommer et al., 2011). The largest values occur at short periods, with amplitudes larger than 2/3 for near-source sites, while at long periods, the ratios are lower than 2/3 close to the fault and tend to increase at longer distances, probably due to the presence of surface waves generated during propagation.

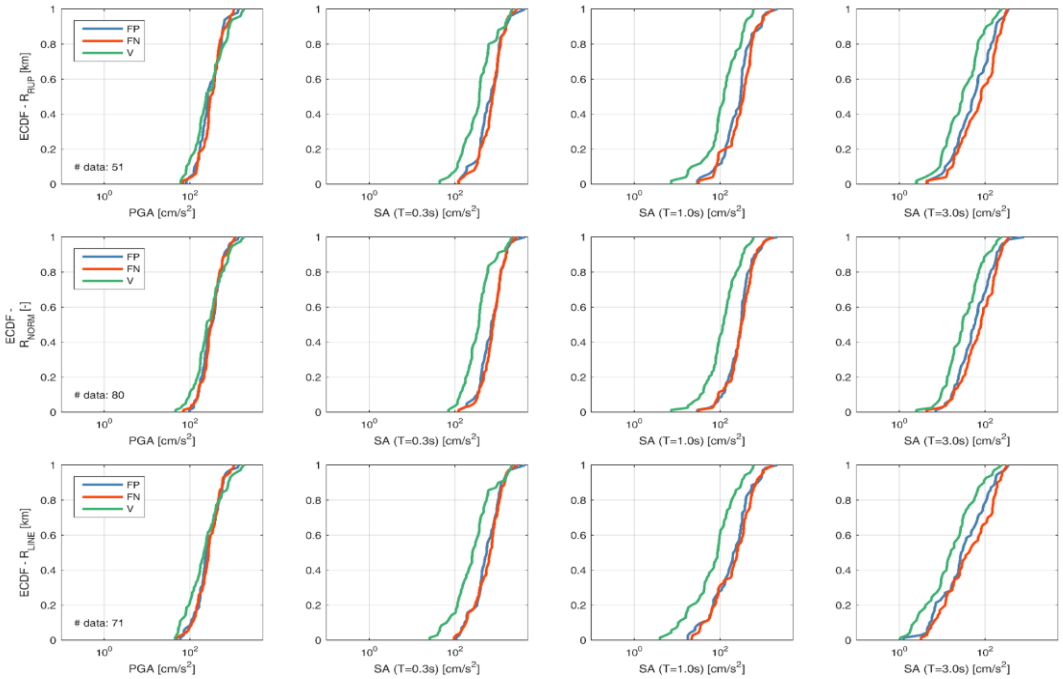

Figure 8. Cumulative distributions of different IMs observed at distances R_{RUP} (top), R_{NORM} (middle) and R_{LINE} (bottom) < 5 km for fault-normal (FN), fault-parallel (FP) and vertical components (V). Number of data for each considered metric is also reported.

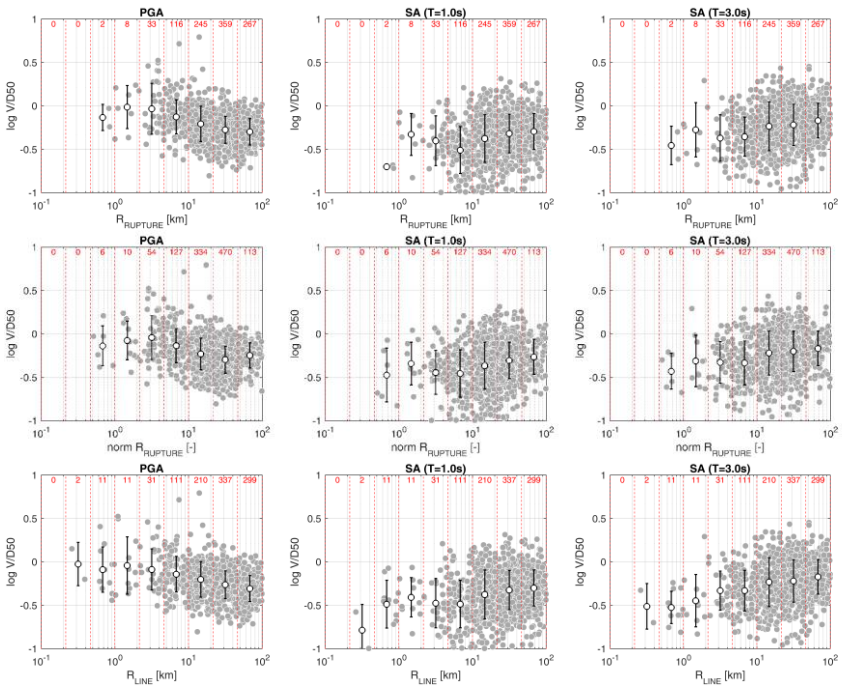

Figure 9. Ratio of Vertical to D50 for three IMs rupture distance (top), normalized rupture distance (middle) and R_{LINE} (bottom).

We also investigate the ratio D100/D50 as a function of distance (Figure 10) and period (Figure 11). As observed by Boore (2011), this ratio never exceeds the 1.42 value corresponding to the value expected for linearly polarized ground motion. As shown in Figure 10, the ratios slightly depend on distance, with largest values close to the fault. This feature, despite distance bins being poorly sampled up to 5 km, might suggest that source contributions, such as radiation pattern and directivity effects, produce polarized ground motions that rapidly vanish with distance.

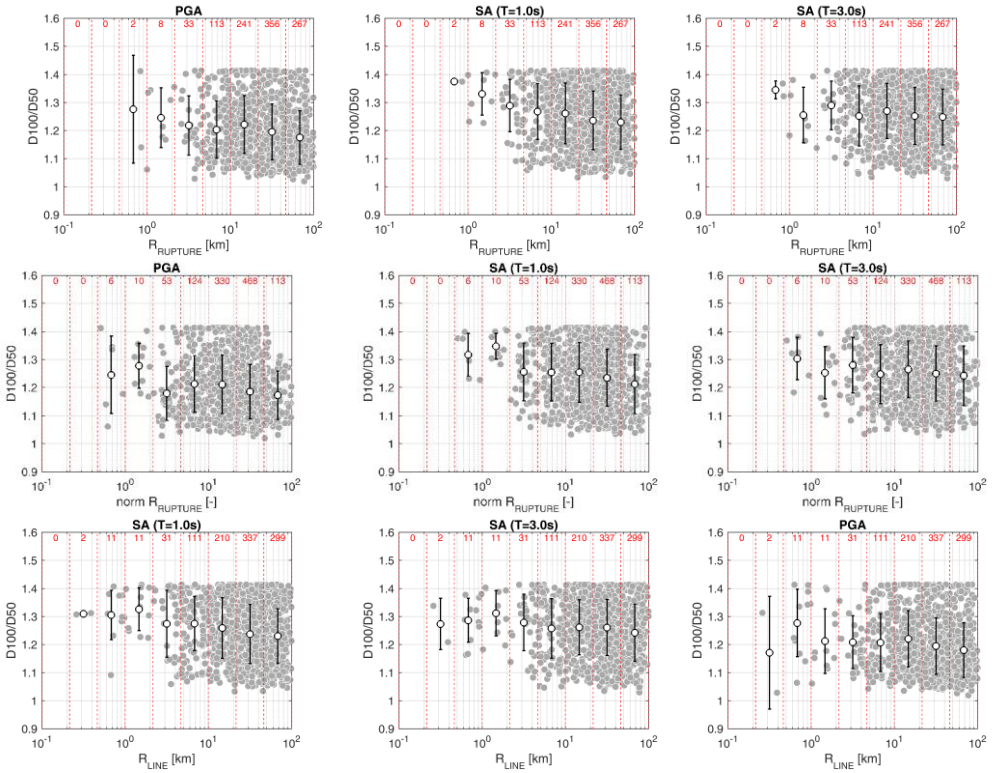

Figure 10. Ratio of D100 to D50 for three IMs versus rupture distance (top) normalized rupture distance (middle) and R_{LINE} (bottom).

Figure 11 shows that the ratios (averaged over all magnitudes) extracted from NSSM05 dataset are in good agreement with other studies (Shahi and Baker, 2014; Boore and Kishida, 2017) up to periods of 6s. At longer periods, the examined ratios increase more slowly than the other models; this is probably due to the presence of analog data, characterized by high-pass cutoff frequency around 0.2 Hz.

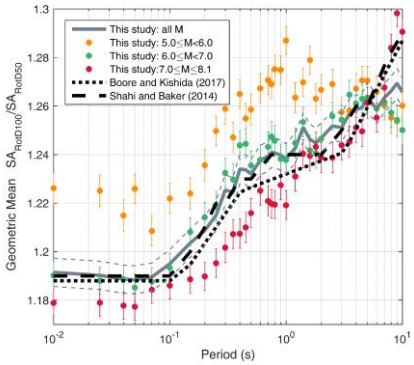

Figure 11. D100/D50 ratios for all records and for three magnitude bins, as well as all magnitude bins combined (all magnitudes, the same as $5 \leq M_w \leq 8$). For each period, the D100/D50 is computed as the geometric mean of the ratios for each observation. The bars represent the 95% confidence of the mean. The NSSM05 data trend is compared with the models of Shahi and Baker (2014) and Boore and Kishida (2017).

Standard deviations normalized by the root square of the number of data (standard error), associated to the median values for FN/FP, V/D100 and D100/D50 are shown in Figure 12 in function of the bin distance for PGA and SA at T = 3s, respectively. The dispersion of data around the median values of the investigated ratios is similar for the considered metrics, suggesting that the spatial distribution of the ground motion in near-source conditions needs further explanatory variables parameters in addition to the distance.

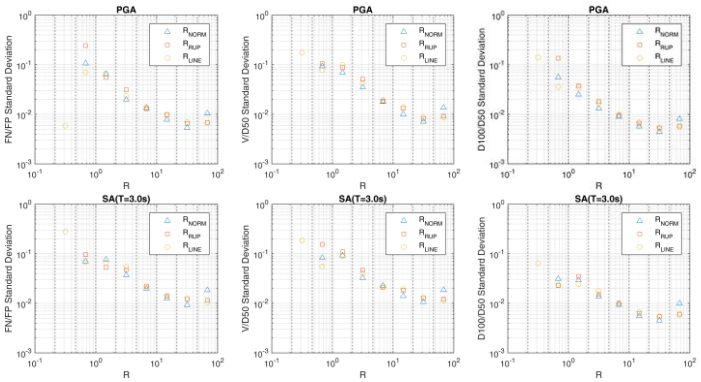

Figure 12. Standard errors, associated to the median values for FN/FP, V/D50 and D100/D50 for PGA (top) and SA (bottom) at T = 3.0 s, plotted in function of the bin distance.

3.2 Pulse-like ground motions

One of the near-source effects that can partly account for the observed polarization of ground motion is the emergence of pulse-like waveforms. These may be the result of rupture directivity leading to a constructive wave interference effect; this appears on the velocity record in the form of a double-sided pulse (Somerville et al., 1997). For the identification of pulse-like ground motions from within the NSSM05 dataset set, the wavelet-transform-based algorithms developed by Baker (2007) and by Shahi and Baker (2014) were used to create a candidate pool of records, from which pulse-like velocity traces were finally identified by visual inspection based on expert judgement. For this analysis, only stations for which information on instrument orientation was available were considered; out of a total of 867 records examined 196 were labeled pulse-like. It should be noted that the pulse-like waveforms identified in this manner may be due to various effects, apart from rupture directivity, such as site response (geotechnical) effects and hanging wall or basin wave-entrapment effects; the pulse-like characterization attributed to some of these ground motions is based on the characteristics of the signal and does not univocally distinguish among these causal effects. Figure 13 provides an example of this characterization in the vicinity of the rupture plane of the 2016 Central Italy sequence's mainshock.

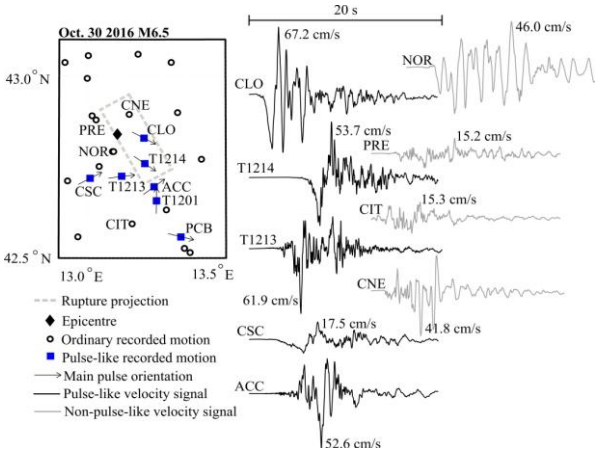

Figure 13. Position of accelerometric stations that recorded pulse-like ground motions plotted over the horizontal projection of the rupture plane, for the 30th Oct. 2016 M_w 6.5 event central Italy sequence (stations with non-pulse like records also shown). Some representative velocity traces of pulse-like (black lines) and non-pulse-like (grey lines) records are shown (common amplitude scale and duration). Orientation of pulse-like components is the one indicated on the map. Adapted from Iervolino et al. (2017).

5. CONCLUSIONS

In this work, we proposed a collection of worldwide near-source accelerometric records, belonging to moderate and strong events with the aim of constructing a flat-file of ground motion parameters and associated metadata and investigating shaking characteristics close to the seismic source. A fundamental step in the compilation of the dataset was to retrieve adequate information about event sources, geometries and rupture mechanisms, in order to calculate different metrics to define the distance from the source to the site.

The Near Strong Motion dataset (named NSSM05), is composed by 1116 manually processed strong motion waveforms (three components) relative to 922 accelerometric stations and 88 events with moment magnitude greater than 5.0 and hypocentral depth shallower than 40 km recorded in the period 1993 – 2016. Various ground motion measures have been computed based on the horizontal components of the selected waveforms, including the geometric mean, the median and the maximum ground motion parameters over all orientations.

The main outcomes of the statistical analysis performed on the NSSM05, are:

1. in agreement with other studies, differences between the fault normal and fault parallel components, in terms of spectral accelerations, are only observed at long periods (T > 1 s) and very close to the fault plane (< 5 km), where FN is, on average, 1.5 FP;
2. the ratio between vertical to median ground motion intensity, in terms of spectral accelerations, is significantly dependent on period and distance, as observed by previous authors (Bozorgnia and Campbell, 2004; Bindi et al., 2011; Bommer et al., 2011); at short distances, the ratio is close to 1 at high frequency and lower than 2/3 at long periods; at longer distances, the trend is reversed and increases/decreases at long and short periods, respectively;
3. the ratio D100/D50 depends on period and the behavior is in agreement with published models; differently from these studies, this ratio shows a slight dependence on distance with the largest values close to the source;
4. the scatter of data around the median values of the investigated ratios is similar for the considered metrics, suggesting that the spatial distribution of the ground motion in near-source conditions needs further explanatory variables parameters in addition to the distance.

6. ACKNOWLEDGMENTS

This study has been partially developed in the framework of the project RS2: Earthquake Simulations and Near-Source Effects under the agreement DPC-ReLUIS 2014-2016. The Authors are grateful to

the project coordinator, Roberto Paolucci, and to Lucia Luzi, coordinator of the European Strong Motion Database, for supporting and encouraging the development of this work.

7. REFERENCES

Aki K., and Richards P.G. (1980). Quantitative Seismology. University Science Books.

Allen T.I., and Wald D.J. (2009). On the use of high-resolution topographic data as a proxy for seismic site conditions (VS30). *Bull. Seismol. Soc. Am.*, 99 (2A) 935–943.

Allmann BP, Shearer PM (2009). Global variations of stress drop for moderate to large earthquakes, *J. of Geoph. Res.*, 114, B01310, doi:10.1029/2008JB005821.

Ancheta T.D., Darragh R.B., Stewart J.P., Seyhan E., Silva W.J., Chiou B.S.J., Wooddell K.E., Graves R.W., Kottke A.R., Boore D.M., Kishida T., Donahue J.R. (2014). NGA-West2 Database. *Earthq Spectra* 30 (3): 989–1005.

Baker J.W. (2007). Quantitative classification of near-fault ground motions using wavelet analysis, *Bull. Seism. Soc. Am.*, 97 (5): 1486-1501.

Bindi, D., F. Pacor, L. Luzi, R. Puglia, M. Massa, G. Ameri, and R. Paolucci (2011). Ground motion prediction equations derived from the Italian strong motion database, *Bull. Seism. Soc. Am.*, 9 1899-1920.

Bommer, J. J., J. Douglas, F. Scherbaum, F. Cotton, H. Bungum, and D. F¨ah (2010). On the Selection of Ground-Motion Prediction Equations for Seismic Hazard Analysis. *Seism. Res. Lett.*, 81, 783–793.

Boore D.M. (2010). Orientation-independent, non geometric-mean measures of seismic intensity from two horizontal components of motion. *Bull. Seismol. Soc. Am.*, 100: 1830–1835

Boore D.M. and Kishida T. (2017). Relations between some horizontal-component ground motion intensity measures used in practice. *Bull. Seismol. Soc. Am.*, 107: 334-343.

Boore D.M., Joyner W.B. and Fumal T.E. (1997). Equations for estimating horizontal response spectra and peak acceleration from western North American earthquakes: A summary of recent work. *Seismol. Res. Lett.*, 68, 128–153.

Bozorgnia, Y., and K. W. Campbell (2004). The vertical-to-horizontal spectral ratio and tentative procedures for developing simplified V/H and vertical design spectra, *J. Earthq. Eng.*, 4, no. 4, 539–561.

Bray JD, Rodriguez-Marek A. (2004) Characterization of forward-directivity ground motions in the near-fault region. *Soil Dyn. and Earth. Eng.*, 24(11):815–828.

Campbell K.W., Bozorgnia Y. (2003) Updated Near-Source Ground-Motion (Attenuation) Relations for the Horizontal and Vertical Components of Peak Ground Acceleration and Acceleration Response Spectra. *Bull. Seismol. Soc. Am.*, 93(1):314–331.

Chioccarelli, E. Iervolino I. (2010) Near-source seismic demand and pulse-like records: a discussion for L'Aquila earthquake. *Earth. Eng. Struct. Dyn.;* 39:1039–1062.

Eurocode 8 (2005): Design of structures for earthquake resistance – Part 1: General rules, seismic actions and rules for buildings. CEN European Committee for Standardization.

Grimaz S. and Malisan P.; (2014) Near field domain effects and their consideration in the international and Italian seismic codes. Boll. Geof. Teor. Appl., vol. 55, n.4, pp. 717-738.

Hanks T.C., and Kanamori H. (1979). A moment magnitude scale. *J. Geoph. Res.*, 84, 2348-2350.

Iervolino I., Baltzopoulos G., Chioccarelli E, Suzuki A. (2017) Seismic actions on structures in the near-source region of the 2016 central Italy sequence. Bulletin of Earthquake Engineering. DOI: 10.1007/s10518-017-0295-3 (article in press).

Kaklamanos, J., Baise, L.G., Boore, D.M. (2011). Estimating unknown input parameters when implementing the NGA ground-motion prediction equations in engineering practice. *Earth. Spectra*, 27 (4), 1219-1235.

Lay T., Wallace T. (1995). Modern Global Seismology. Academic Press, 521 pp.

Luzi L, Pacor F, Puglia R (2016). Italian Accelerometric Archive v 2.1. Istituto Nazionale di Geofisica e Vulcanologia, Dipartimento della Protezione Civile Nazionale. doi: 10.13127/ITACA/2.1.

Luzi L, Puglia R, Russo E & ORFEUS WG5 (2016). Engineering Strong Motion Database, version 1.0. Istituto Nazionale di Geofisica e Vulcanologia, Observatories & Research Facilities for European Seismology. doi: 10.13127/ESM

Mai M., Thingbaijam K.K.S. (2014). SRCMOD: An Online Database of Finite-Fault Rupture Models. Seismological Research Letters 85 (6) 1348-1357, doi: 10.1785/0220140077.

Mavroeidis GP, Papageorgiou AS. (2003) A mathematical representation of near-fault ground motions. *Bull.*

Seismol. Soc. Am.; 93(3):1099–1131.

Pacor F., Paolucci R., Luzi L., Sabetta F., Spinelli A., Gorini A., Nicoletti M., Marcucci S., Filippi L., Dolce M. (2011). Overview of the Italian strong motion database ITACA 1.0. *Bull Earthquake Eng* 9 (6): 1723–1739. doi: 10.1007/s10518-011-9327-6.

Paolucci R., Pacor F., Puglia R., Ameri G., Cauzzi C., Massa M. (2011). Record processing in ITACA, the new Italian strong-motion database, in Earthquake Data in Engineering Seismology—Predictive Models, Data Management and Networks, S. Akkar, P. Gülkan, and T. van Eck (Editors), Springer, Dordrecht, Netherlands, 99–113, ISBN: 978-94-007-0151-9 (printed version) 978-94-007-0152-6 (e-book version).

Shahi S., J. W. Baker (2014). An Efficient Algorithm to Identify Strong-Velocity Pulses in Multicomponent Ground Motions – Bull Seism. Soc. Am.: Vol. 104, No. 5, pp. 2456-2466.

Somerville PG. (2003) Magnitude scaling of the near fault rupture directivity pulse. *Physics of the Earth and Planetary Interiors*; 137:201–212.

Wald D.J., and Allen T.I. (2007). Topographic slope as a proxy for seismic site conditions and amplification. *Bull. Seismol. Soc. Am.,* 97 (5), 1379-1395.

Wells D.L., and Coppersmith K.J. (1994). New empirical relationships among magnitude, rupture length, rupture width, rupture area, and surface displacement. *Bull. Seismol. Soc. Am.*, 84 (4), 974-1002.

Zevenbergen L.W., and Thorne C.R. (1987). Quantitative analysis of land surface topography. *Earth surface processes and landforms*, 12 (1), 47-56.